

Contents lists available at ScienceDirect

Journal of Quantitative Spectroscopy & Radiative Transfer

journal homepage: www.elsevier.com/locate/jqsrt



Improved δ -Eddington approximation for optically thin clouds

Tong Ren^{a,*}, Ping Yang^a, Guanglin Tang^a, Xianglei Huang^b, Eli Mlawer^c

- ^a Department of Atmospheric Sciences, Texas A&M University, College Station, TX, United States
- ^b Department of Climate and Space Sciences and Engineering, University of Michigan, Ann Arbor, MI, United States
- ^c Atmospheric and Environmental Research, Lexington, MA, United States



ARTICLE INFO

Article history:
Received 15 June 2019
Revised 11 October 2019
Accepted 13 October 2019
Available online 15 October 2019

Keywords: δ -Eddington approximation Forward fraction of scattering The asymmetry factor

ABSTRACT

The δ -Eddington simulations of broadband shortwave net radiation fluxes at the top of the atmosphere (F_{TOA}) and the surface (F_{SURF}) are evaluated with different parameterizations of the forward fraction of scattering (f), including the square of the asymmetry factor ($f=g^2$), the fraction of the forward singlescattered intensity over the total single-scattered intensity ($f = f_p$), and the cube of the asymmetry factor $(f=g^3)$. g^2 and g^3 are respectively the 2nd and 3rd moments of the Henyey-Greenstein (HG) phase function and hence approximate measures of the variance and skewness of the phase function. The factor f_p for spherical droplets is estimated using a truncation angle, which separates the forward peak and diffusive portions of a highly anisotropic phase function. The results show that the simulations of F_{TOA} and F_{SURF} are not improved, if the conventional approach $f = g^2$ is replaced by $f = f_p$ in the δ -Eddington approximation for an atmosphere in the presence of liquid clouds. For the optically thick conditions, multiple scattering plays a dominant role in determining the reflectance (R) and transmittance (T) of the cloudy layer; the conventional parameterization $f = g^2$ is most accurate among the three parameterizations. For the optically thin conditions, single scattering dominates over multiple scattering and thus $f=g^2$ results in biased F_{TOA} and F_{SURF} calculations, particularly with low solar elevations. For such cases, $f=g^3$ shows most accurate F_{TOA} and F_{SURF} results for both liquid and ice clouds, though $f=g^3$ also results in smaller cloud layer heating rates in general.

© 2019 Elsevier Ltd. All rights reserved.

1. Introduction

The scattering of sunlight by atmospheric particles, such as cloud water droplets, ice particles, and aerosol particles, can be highly anisotropic and complex (e.g., [1-5]), which makes accurate modeling of such processes computationally expensive. Many applications such as in general circulation models (GCMs) require rapid and reasonably accurate calculations of solar fluxes and heating rates through the entire atmosphere; as a result, the radiative transfer equation must be solved with certain analytical approximations. Among the various approximations, the two-stream approximation (assuming only one downward beam and one upward beam) and its variants [2] have been extensively used. One shortcoming of two-stream approximation is the handling of highly asymmetric phase functions [1], as in the case of cloud particles and coarse-mode dust aerosols in the atmosphere. Therefore, the two-component method has been introduced in estimations of radiative fluxes, where the highly strong peak of forward scattering is treated as the Dirac delta function (δ) and separated from the diffusive portion of the phase function [1,6]. When the truncated diffusive part takes the form of the Eddington approximation [7], the two-component method is called the δ -Eddington approximation [1]. When the truncated diffusive part uses more than two terms of the associated Legendre expansion [8], the two-component method is the called δ -M approximation [6]. The replacement of the forward scattering peak by the delta function results in scaled optical parameters, and hence this method is also called the δ -scaling approach. Joseph et al. [1] also show the equivalence between the δ -scaling approach and the similarity principle (e.g. [9]).

The δ -Eddington approximation and other δ -scaling two-stream methods (e.g., [10]) have been widely used in GCM radiation schemes [11–13]. The δ -scaling two-stream methods are generally more accurate than the conventional two-stream methods [14]. By comparing different two-stream methods under a variety of conditions, King and Harshvardhan [15] concluded that no single method is always adequately accurate in various solar zenith angle and optical thickness regimes, but the δ -Eddington approximation may be the most suitable for GCMs due to its reasonble accuracy for moderately thick cloud layers over a wide range of solar zenith angles. However, previous studies also reported persistent biases

^{*} Corresponding author. E-mail address: tr7585@tamu.edu (T. Ren).

introduced by the δ -scaling two-stream GCM approximations in aerosol radiative forcing [13] and surface net shortwave flux [14].

The parameterization of the forward scattering fraction (f) in the δ -Eddington approximation [14,16,17] can contribute to the radiation flux uncertainties. The δ -scaling approach results in a scaled asymmetry factor (g) that represents the asymmetry of the diffusive part of the phase function; gis smaller than the original asymmetry factor (g). Moreover, gdecreases with increasing f. In other words, the diffusive part of the phase function is less asymmetric with increasing f. When the δ -scaling approach was introduced, Joseph et al. [1] suggested f be set to g^2 , the 2nd moment of the Henyey-Greenstein (HG) phase function, making the δ -Eddington and HG phase functions agree up to three terms. The 2nd moment is related to the variance of the phase function. However, it is challenging to figure out and remains unclear how fshould be parameterized in order to provide the best accuracy of the δ -Eddington approximation [17]. Later studies tried different empirical parameterizations of f [14,16,17]. Li [16] parameterized f as a function of g, solar zenith angle (θ_0), and single-scattering albedo (ω) and showed improved results in non-conservative (ω < 1) cases with small θ_0 and in optically thin conservative ($\omega = 1$) cases. Qiu [17] parameterized f as a function of g, θ_0 , ω , optical thickness (τ), and surface reflectance and showed significantly improved results in the condition of $\tau \leq 1$. Räisänen [14] parameterized f separately for water clouds, ice clouds, and aerosols and showed significantly improved flux simulations based on GCM experiments, particularly with low solar elevations. In the study by Räisänen [14], f is set to the cube of the asymmetry factor (g^3) for aerosols, which generally have a relatively small τ . The cube of the asymmetry factor (g^3) is the 3rd moment of the HG phase function, which is related to the skewness of the phase function.

Recent studies [18,19] applied the small-angle approximation (SAA; e.g., [20] and references therein) in the two-component method for solving the angular distribution of radiance. Instead of approximating the forward scattering peak in terms of the delta function, Sun et al. [19] characterize the forward scattering component by an exponential function of the scattering angle (Θ) , where an approximate analytical solution of the forward radiance can be obtained using the SAA; a truncation angle (Θ_c) is selected to separate the forward and diffusive components of the phase function, and the forward fraction of single-scattering (f_{TA}) is estimated. In Sun et al. [19], the radiance angular distribution of the diffusive component is solved using the successive order of scattering (SOS) method, which has a computational time proportional to τ [21–24]. Consequently, although the combined SAA+SOS method in Sun et al. [19] provides an improved angular distribution of radiance, this method is expensive for optically thick conditions. Hereinafter, we refer the combined SAA + SOS method in Sun et al. [19] as truncation angle method.

If only the upward and downward radiative fluxes are to be solved, to the best of our knowledge, it remains unclear whether the estimation of f_{TA} using Θ_c [19] can be used to parameterize f in the computationally efficient δ -scaling two-stream methods. The separation of forward and diffusive components using Θ_c also provides a way of evaluating the ratio of forward singlescattered intensity over total single-scattered intensity (f_p). In addition to f_{TA} and f_p , the phase function skewness is also a measure of the asymmetry of the phase function. It also remains unclear whether δ -scaling two-stream methods will show better accuracy if f_p or some measure of the phase function skewness is used in the parameterization of f. Therefore, the objectives of this study include: (1) finding a way of choosing Θ_c ; (2) parameterizing f_{TA} and f_p as functions of effective radius (r_{eff}); and (3) examining the performance of $f=f_{\rm g2}=g^2$, $f=f_{\rm TA}$, $f=f_p$, and $f=f_{\rm g3}=g^3$ in the δ -Eddington approximation in terms of the radiation fluxes at the top of the atmosphere (TOA; F_{TOA}) and the surface (F_{SURF}). The parameterizations of f are tested through the simulations in overcast conditions of liquid clouds. If any parameterization shows improved F_{TOA} and F_{SURF} , then this parameterization is further tested in overcast ice cloud conditions. Section 2 introduces the methods and radiative transfer models used in this study. Simulations results with different parameterizations of f are presented in Section 3, followed by conclusions in Section 4.

2. Methodology

2.1. Two-component method

Both the δ -scaling and truncation angle approaches start with the two-component method, in which the phase function (p) is approximated as a linear combination of the forward peak and diffusive components:

$$p(\chi) = 2f\delta(1-\chi) + (1-f)p_s(\chi),\tag{1}$$

where χ is the cosine of the scattering angle ($\chi = \cos\Theta$) and $p_s(\chi)$ is the scaled phase function. In the δ -Eddington approximation, $p_s(\chi) = \omega(1+3 \text{ g}'\chi)$, where gis the scaled asymmetry factor of the diffusive component [1]. The phase function decomposition [19] in the truncation angle approach

$$p(\chi) = f_{TA} p^f(\chi) + (1 - f_{TA}) p^d(\chi)$$
 (2)

can be obtained by letting

$$\begin{cases} f = f_{TA} \\ 2\delta(1-\chi) = p^f(\chi) \\ p_s(\chi) = p^d(\chi) \end{cases}$$
 (3)

in Eq. (1), where the forward and diffusive phase function components $p^f(\chi)$ and $p^d(\chi)$ are given by

$$p^{f}(\chi) = \frac{1}{f_{TA}} \begin{cases} p(\chi) - p(\chi_c) exp[-(\chi - \chi_c)/n_{ph}(1 - \chi_c)], & \chi \geq \chi_c \\ 0, & \chi < \chi_c \end{cases}$$
(4)

$$p^{d}(\chi) = \frac{1}{1 - f_{TA}} \begin{cases} p(\chi_{c}) exp[-(\chi - \chi_{c})/n_{ph}(1 - \chi_{c})], & \chi \geq \chi_{c} \\ p(\chi), & \chi < \chi_{c} \end{cases}$$
(5)

and the forward fraction of single-scattering f_{TA} is given by

$$f_{TA} = \frac{1}{2} \int_{\chi_c}^{1} \left\{ p(\chi) - p(\chi_c) exp \left[-(\chi - \chi_c) / n_{ph} (1 - \chi_c) \right] \right\} d\chi, \quad (6)$$

satisfying

$$\frac{1}{2} \int_{-1}^{1} p^{f,d}(\chi) d\chi = 1. \tag{7}$$

The continuity of the derivative of $p^d(\chi)$ or $p^f(\chi)$ at the truncation angle $\chi = \chi_c = \cos\Theta_c$ requires

$$n_{ph} = -\frac{p(\chi_c)}{p'(\chi_c)(1-\chi_c)},\tag{8}$$

where $p(\chi_c)$ is the derivative of phase function at the truncation angle χ_c .

In the two-stream approximations, the analytical solutions of the reflectance (R) and transmittance (T) of an atmospheric layer are functions of τ , ω , and g [2]. The δ -scaling method transforms τ , ω , and g into scaled values:

$$\begin{cases} \tau' = (1 - \omega f)\tau \\ \omega' = (1 - f)\omega/(1 - \omega f), \\ g' = (g - f)/(1 - f) \end{cases}$$
 (9)

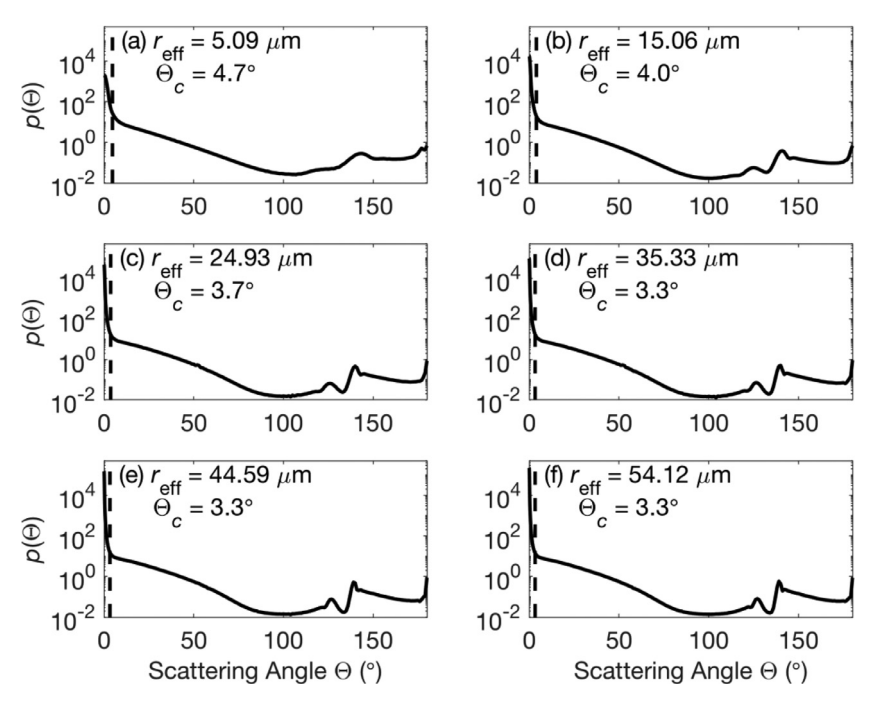


Fig. 1. Phase functions $p(\Theta)$ at 0.532 μ m for 6 selected gamma size distributions of water droplets that have effective radii of 5.09, 15.06, 24.93, 35.33, 44.59, and 54.12 μ m, respectively. In each panel, the dashed line marks the associated truncation angle (Θ_c) .

where τ_i ω_i and gare the scaled optical thickness, single-scattering albedo, and asymmetry factor, respectively [1]. The three parameters are functions of f only. Consequently, the modification of R and T by the δ -scaling method depends only on how the forward fraction of scattering f is parameterized in the two-stream approximations. Due to the phase function decomposition analogy between the δ -scaling and truncation angle methods Eqs. (1)–(3), the evaluation of f_{TA} in the truncation angle method Eq. (6) may be used to parameterize f in the δ -scaling method by setting f= f_{TA} .

2.2. Selection of truncation angle

In the truncation angle method, the motivation of selection of a truncation angle is to most appropriately separate the sharp forward peak scattering from the diffusive scattering, where the scattered intensity varies smoothly with the scattering angle [19]. In addition, given a particle size distribution, the phase function of the particles varies with of the wavelength of the incident light. Hence, we suggest that a truncation angle $\Theta_{\mathcal{C}}$ may be defined as the angle Θ , where the change of the derivative of phase function starts to become "slow" at a certain wavelength:

$$\left| \frac{\partial}{\partial \Theta} \left(\frac{\partial p(\chi)}{\partial \chi} \right) \right|_{\Theta \ge \Theta_c} < \frac{180}{\pi} c_0 \frac{\lambda}{\lambda_0}, \tag{10}$$

where λ is wavelength; c_0 is an empirical constant that may be subjectively selected to define how slow the derivative is considered as "slow" at the wavelength λ_0 . We subjectively choose $c_0=10^4$ at $\lambda_0=0.532~\mu\mathrm{m}$ and test the choice c_0 at any other wavelength λ using the phase functions of spherical water droplets with different effective radii (r_{eff}). The precision of Θ_c determined through criterion (10) is limited by the selected angles where phase functions and their derivatives are evaluated. We let Θ_c take angles with one decimal digit.

Based on the Morrison microphysics scheme, a gamma size distribution of spherical water droplets is assumed [25]. This study uses that empirical relationship between the relative radius dispersion and the water droplet number concentration [25,26] to gener-

ate 82 gamma size distributions whose effective radii range from 2.53 to $58.49\,\mu\text{m}$. The water droplet number concentration is fixed to $100~\text{cm}^{-3}$ and 82 liquid water content (LWC; kg m⁻³) values are selected in generating the distributions. Then, the Lorenz–Mie scattering program [27] is used to calculate the phase function at $0.532\,\mu\text{m}$ for each generated gamma size distribution of spherical water droplets. The complex refractive index of water at $0.532\,\mu\text{m}$ is taken from Hale and Querry [28]. The truncation angles found for the 82 phase functions range from 3.3° to 5.0° Fig. 1 shows that the larger a water droplet is, the stronger the forward peak scattering is and the smaller the truncation angle is.

Once Θ_c is determined, f_{TA} can be calculated using the Eq. (6). In addition, the ratio of forward single-scattered intensity over total single-scattered intensity (f_p) can be estimated through the following equation:

$$f_{p} = \frac{\int_{0}^{\Theta_{c}} p(\Theta) \sin(\Theta) d\Theta}{\int_{0}^{\pi} p(\Theta) \sin(\Theta) d\Theta} = \frac{1}{2} \int_{0}^{\Theta_{c}} p(\Theta) \sin(\Theta) d\Theta. \tag{11}$$

As shown in Fig. 2, it appears both f_{TA} and f_p are smaller than $f_{g2}(=g^2)$ and $f_{g3}(=g^3)$ in the δ -scaling approach; f_{TA} and f_p are closer to f_{g3} than to f_{g2} , i.e. $f_{g2} > f_{g3} > f_{TA}$ (or f_p). The results suggest that $g(f=f_{g2}) < g(f=f_{g3}) < g(f=f_{TA})$ or f_p . In other words, the diffusive part of the phase function is least asymmetric if $f=f_{g2}$ and most asymmetric if $f=f_{TA}$ or f_p at 0.532 μ m. As r_{eff} increases from 2.53 to 58.49 μ m, f_{TA} increases from 0.180 to 0.494, f_p increases from 0.378 to 0.499, f_{g3} increases from 0.573 to 0.683, and f_{g2} increases from 0.690 to 0.776. When the size parameter $(a=2\pi r_{eff}/\lambda)$ is adequately large, the forward single-scattered intensity is always about half of the total single-scattered intensity, i.e. $f_p \approx 0.500$, which is not sensitive to small variations of Θ_c (not shown). Actually, the forward diffraction of particles with a large size parameter is approximately half of the total incident energy (e.g., [29]).

Previous parameterization studies suggested that the bulk optical properties of water and ice clouds—such as the extinction coefficient ($\beta_{\rm ext}$), ω , and g—are more sensitive to the effective particle

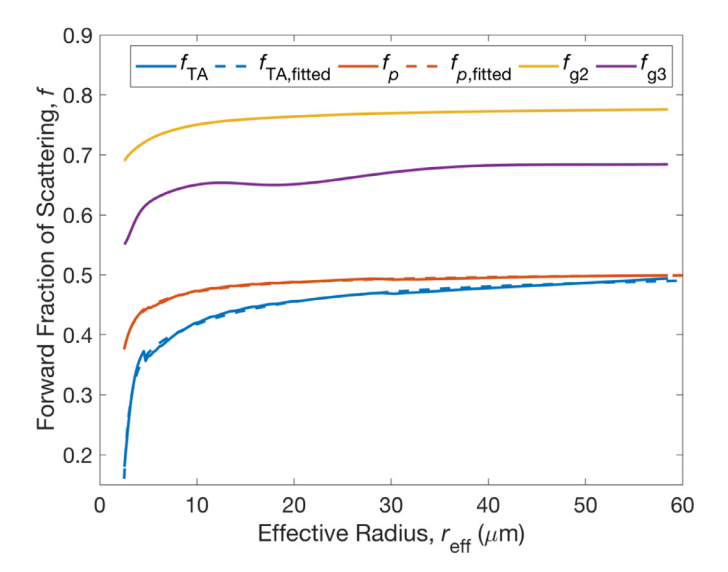


Fig. 2. Forward fraction of scattering (f) of cloud water droplets parameterized using the 2nd ($f_{g2} = g^2$) and 3rd ($f_{g3} = g^3$) moments of the HG phase function, the truncation angle approach (f_{TA}), and the ratio of forward single-scattered intensity to the total single-scattered intensity (f_p) at a wavelength of 0.532 μ m. The dashed curves are fitted f_{TA} and f_p lines using Eq. (12).

size than to the shape of the size distribution of water droplets or ice particles [30–32]. In this study, we parameterize $f_{\rm TA}$ and f_p as 3rd-order polynomials of the inverse of $r_{\rm eff}$:

$$\begin{cases} f_{\text{TA,fitted}} = \alpha_0 + \frac{\alpha_{-1}}{r_{\text{eff}}} + \frac{\alpha_{-2}}{r_{\text{eff}}^2} + \frac{\alpha_{-3}}{r_{\text{eff}}^2} \\ f_{p,\text{fitted}} = \beta_0 + \frac{\beta_{-1}}{r_{\text{eff}}} + \frac{\beta_{-1}}{r_{\text{eff}}^2} + \frac{\beta_{-3}}{r_{\text{eff}}^3} \end{cases}, \tag{12}$$

where the coefficients α_i and β_i (i=0,-1,-2,-3) may be determined in a least-square sense. As shown in Fig. 2, this parameterization (12) provides a best fit of $f_{\rm TA}$ and f_p . The discontinuities on the $f_{\rm TA}$ and f_p curves shown in Fig. 2 result from the discretization of the tested values of Θ_c through criterion (10). For example, when $r_{\rm eff}$ increases from 4.53 $\mu{\rm m}$ to 4.71 $\mu{\rm m}$, Θ_c decreases from 5.0° to 4.8°. However, these discontinuities of $f_{\rm TA}$ and f_p with respect to $r_{\rm eff}$ shown in Fig. 2 do not affect the results and conclusions of this study and are basically compensated for by using the fitted values of $f_{\rm TA}$ and f_p .

Another 389 gamma size distributions of spherical water droplets are generated by letting both droplet number concentration and LWC take random numbers, making the shapes of the new

389 size distributions different from the 82 ones used to fit the coefficients α_i and β_i (i=0, -1, -2, -3) in Eq. (12). As shown in Fig. 3, $f_{\text{TA},\text{fitted}}$ and $f_{p,\text{fitted}}$ generally overestimate f_{TA} and f_{p} , respectively. The parameterization in Eq. (12) of f_{TA} and f_{p} show small RMSEs of 0.011 and 0.006, respectively, for the 389 new randomly generated size distributions, suggesting that f_{TA} and f_{p} are more sensitive to the effective radius than the shape of the gamma size distribution of the spherical water droplets.

2.3. Model configuration

The parameterization in Eq. (12) provides a chance to compare the difference of the two-component methods with $f_{\mathrm{TA,fitted}}$, $f_{p,\mathrm{fitted}}$, $f_{\rm g3}$, and $f_{\rm g2}$ in net radiation fluxes at the TOA ($F_{\rm TOA}$) and the surface (F_{SURF}). The δ -Eddington method is adopted for the comparison. The Rapid Radiative Transfer Model (RRTM) shortwave model (RRTM_SW; [33]) and its simplified version for GCMs (RRTMG_SW; [34,35]) are used for this comparative study. The RRTMG_SW has been applied in both global and regional models, such as the Community Earth System Model (CESM; [36]) and the Weather Research and Forecasting (WRF) model [37,38]. In RRTM_SW, multiple scattering is treated using the δ -M scaling approach [6], which combines δ -scaling [1] and the Discrete Ordinate Radiative Transfer model (DISORT; e.g., [39,40]). This is more accurate than the two-stream approximations in the RRTMG_SW. We therefore take RRTM_SW as the reference model and use the RRTMG_SW to test the performance of the two-stream approximations with the forward fractions of scattering (f) parameterized in different ways (i.e.

 $f=f_{\text{TA,fitted}}, f=f_{p,\text{fitted}}, f=f_{\text{g3}}=g^3$, and $f=f_{\text{g2}}=g^2$). The shortwave spectrum wavenumbers between 820 and 50,000 cm⁻¹ (or $\lambda=0.200$ and 12.2 µm) is divided into 14 bands (Bands 16–29) based on the absorption features of the primary and minor atmospheric species in the RRTM_SW/RRTMG_SW (Fig. 4; [33]). The refractive index dataset of water by Hale and Querry [28] is used to calculate the phase functions of spherical water droplets with a gamma size distribution for each of the 14 bands. For each band, the phase functions associated with all the wavelengths in this band where refractive indices are available are calculated using the Lorenz–Mie program [27]. Then, the mean phase function for each band $p_{\text{Bandi}}(\Theta, r_{\text{eff}})$ is estimated by averaging the phase functions at the available wavelengths $p_{\lambda i}(\Theta, r_{\text{eff}})$ within this band using the scattering cross sections $C_{\text{Sca},\lambda i}$ as the weights (Fig. 5):

$$p_{Bandi}(\Theta, r_{\text{eff}}) = \frac{\sum_{i} p_{\lambda i}(\Theta, r_{\text{eff}}) C_{sca, \lambda i}}{\sum_{i} C_{sca, \lambda i}}.$$
 (13)

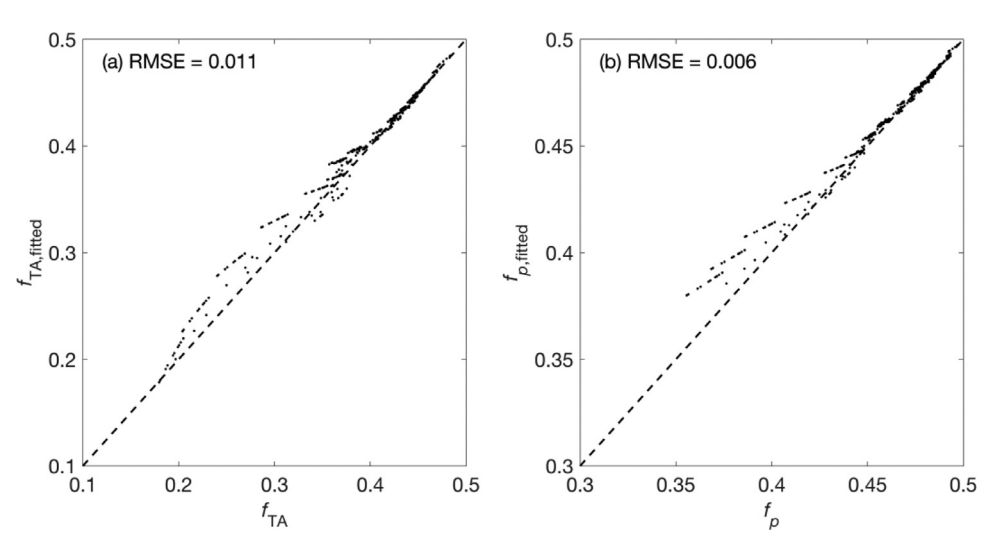


Fig. 3. Scatterplots at $0.532 \, \mu \text{m}$ of (a) $f_{\text{TA,fitted}}$ vs. f_{TA} (b) and $f_{p,\text{fitted}}$ vs. f_p , using 389 randomly generated gamma size distributions of spherical water droplets.

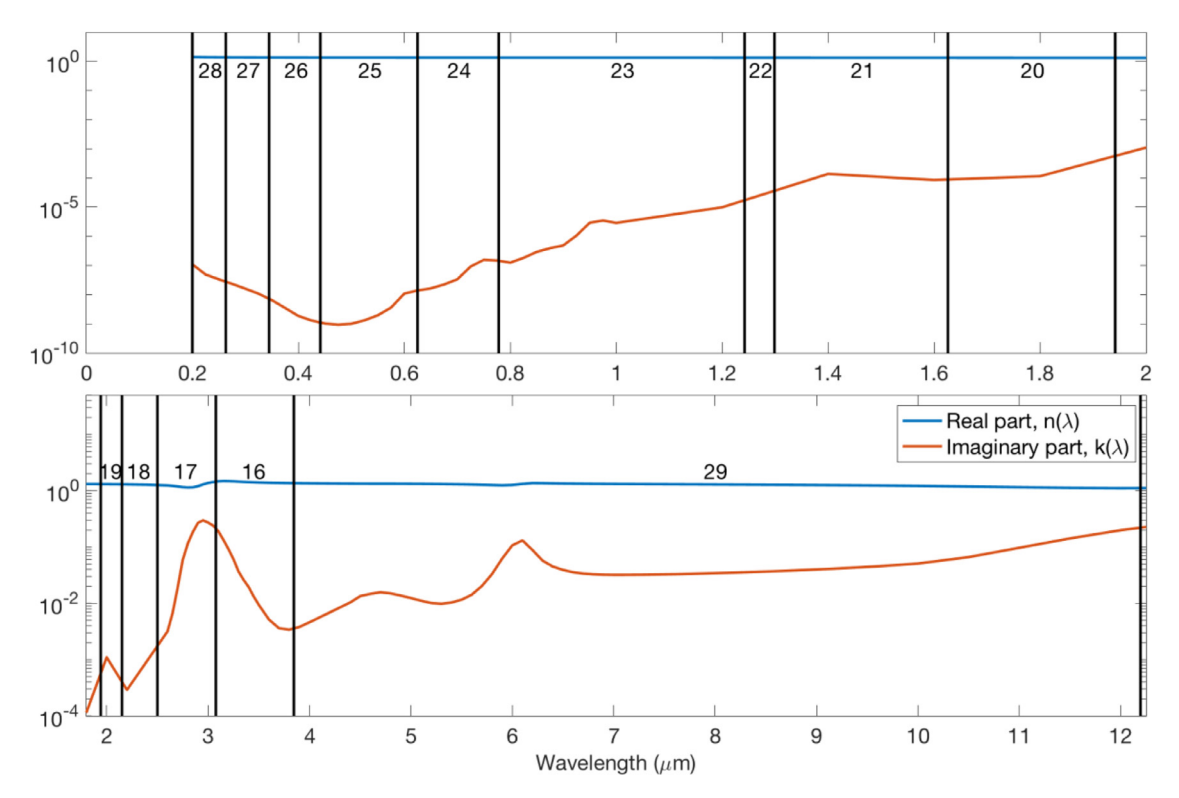


Fig. 4. The real and imaginary parts of the refractive index of water [28] in the shortwave region with the RRTM_SW/RRTMG_SW band divisions (Bands 16-29).

Band 22 is so narrow that no refractive index from this dataset is available within the band and in that band the refractive index is linearly interpolated between the two nearest available wavelengths.

After the mean phase functions for all 14 bands $p_{\text{Bandi}}(\Theta, r_{\text{eff}})$ (i = 16, 17,..., 29) are obtained, criterion (10) is applied to all the phase functions to get their truncation angles. Then, Eqs. (6) and (11) are used to derive f_{TA} and f_p for each band. In the longer wavelength regime (Bands 16, 17, and 29), f_p is generally greater than 0.5. Eq. (12) are then used to parameterize f_{TA} and f_p for each of the 14 bands, where the coefficients α_i and β_i (i = 0, -1, -2,-3) are fitted in a least-square sense. In the infrared bands (Bands 16-22 and 29), the forward scattering is not strong for smaller particle sizes, and therefore no truncation angle can be found through the criterion (10). For such cases, we find a smallest r_0 such that truncation angles can be found through the criterion (10) for all the gamma size distributions whose effective radii are greater than r_0 . Then, we assume f_{TA} and f_p equal to 0 for 2.50 μ m $\leq r_{eff} < r_0$, meaning the scaling of τ , ω , and g (Eq. (9)) is not necessary for the spherical water droplets that have small effective radii for these bands (Bands 16-22 and 29). Eq. (12) are applied to parameterize f_{TA} and f_p for $r_0 \le r_{\text{eff}} \le 60.00 \,\mu\text{m}$, namely

$$f_{\text{TA,fitted}} = \begin{cases} 0, & 2.50 \ \mu m \le r_{\text{eff}} < r_0 \\ \alpha_0 + \frac{\alpha_{-1}}{r_{\text{eff}}} + \frac{\alpha_{-2}}{r_{\text{eff}}^2} + \frac{\alpha_{-3}}{r_{\text{eff}}^3}, & r_0 \le r_{\text{eff}} \le 60.00 \ \mu m, \end{cases}$$
(14)

$$f_{p,\text{fitted}} = \begin{cases} 0, & 2.50 \,\mu\text{m} \le r_{\text{eff}} < r_0 \\ \beta_0 + \frac{\beta_{-1}}{r_{\text{eff}}} + \frac{\beta_{-2}}{r_{\text{eff}}^2} + \frac{\beta_{-3}}{r_{\text{eff}}^3}, & r_0 \le r_{\text{eff}} \le 60.00 \,\mu\text{m}, \end{cases}$$
(15)

where r_0 is the smallest effect radius at which a truncation angle can be found through the criterion (10). For bands 16–22, r_0 = 7.21, 6.17, 5.50, 4.89, 4.53, 3.88, and 3.45 μ m, respectively; for bands 23–28, r_0 = 2.53 μ m; for band 29, r_0 = 10.22 μ m. The parameterizations of f_{TA} and f_p in the 14 bands are incorporated in the RRTMG_SW. Then, δ -Eddington simulations of radiation fluxes at

the TOA and surface are conducted using the RRTMG_SW with the forward fraction of scattering f parameterized by $f_{\text{TA,fitted}}$, $f_{p,\text{fitted}}$, $(f_{\text{g3}} = g^3)$, and $(f_{\text{g2}} = g^2)$ respectively, for a comparison. The results are presented in the next section.

3. Results

3.1. Comparison of f_{g2} , $f_{p,fitted}$, and f_{g3}

As stated in Section 2.3, the treatment of multiple scattering using DISORT is more accurate than using the two-component methods, and hence DISORT has been widely used as the reference model to test the performance of more simplified methods (e.g., [14,41,42]). Tang et al. [42] used the 16-stream DISORT (8 downward and 8 upward beams) as the reference model to examine faster radiation schemes [43,44] of the cloud longwave scattering in terms of the longwave broadband irradiance. Turner [45] and Turner et al. [46] used the 16-stream DISORT to determine cloud phase (water, ice, or mixed water and ice) based on the measurements from the Atmospheric Emitted Radiance Interferometer (AERI). The RRTM_SW with the δ -16-stream DISORT configuration is therefore adopted as the reference model in this study.

As documented in Table 1, a number (62,640) of conditions are selected to compare the irradiances at the TOA (F_{TOA}) and the surface (F_{SURF}) with $f=f_{TA,fitted}$, $f_{p,fitted}$, f_{g3} , and f_{g2} in the optically thin (CWP=20 g m⁻²) and thick (CWP=200 g m⁻²) regimes. The parameterization by Hu and Stamnes [31] is divided into 3 different radii intervals, 2.5–12 μ m, 12–30 μ m, and 30–60 μ m, bringing discontinuous features of simulated F_{TOA} and F_{SURF} near the boundaries of the radii intervals (not shown). Therefore, we do not use the Hu and Stamnes [31], but we compute look-up-tables (LUTs) of the bulk optical properties in each of the 14 RRTM_SW/RRTMG_SW bands using the Lorenz–Mie scattering program [27]. The LUTs provide extinction coefficient ($\beta_{\rm ext}$), ω , and g for 58 gamma size distributions that have effective radii from 2.5 to 59.5 μ m with an

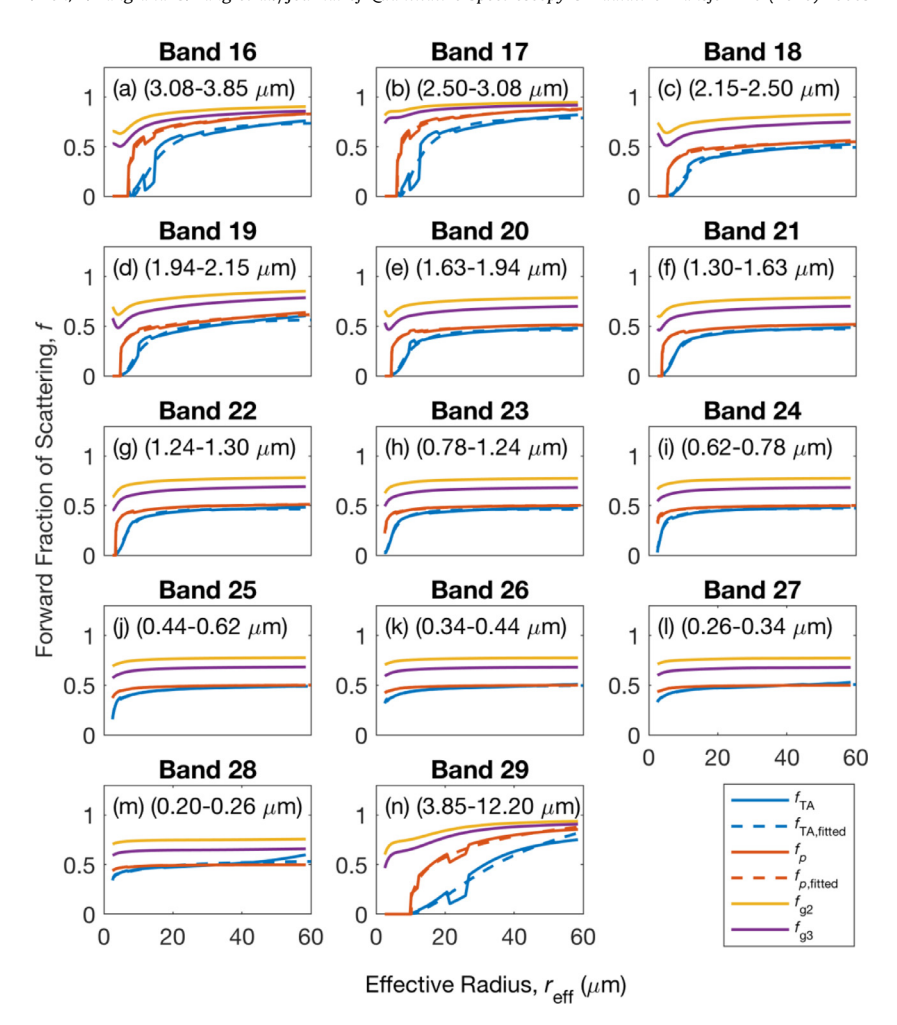


Fig. 5. Forward fraction of scattering (f) of cloud water droplets for the 14 RRTM_SW/RRTMG_SW bands parameterized using the 2nd ($f_{g2} = g^2$) and 3rd ($f_{g3} = g^3$) moments of the HG phase function, the truncation angle approach (f_{TA}), and the ratio of forward single-scattered intensity to total single-scattered intensity (f_p). The dashed curves in each panel are the fitted f_{TA} and f_p using Eq. (12). The wavelength interval in the parenthesis in each panel is the bandwidth of that band.

 Table 1

 Selected conditions for the comparison simulations.

RRTMG_SW/RRTM_SW input parameters	Selected values (or options)			
Atmospheric profiles	U.S. Standard Atmosphere, 1976			
•	Tropical			
	Midlatitude summer			
	Midlatitude winter			
	Subarctic summer			
	Subarctic winter			
Parameterization	Lorenz-Mie-based LUTs			
Cloud layer height (km)	Between 1.75 and 2.00 km			
Cloud water paths (CWP; g m ⁻²)	20 and 200			
Solar zenith angles, θ_0 (°)	From 0.5 to 89.5 with an increment of			
-	1.0			
Effective radii, $r_{\rm eff}$ (μ m)	From 2.5 to 59.5 with an increment of			
	1.0			
Surface albedo	0.2			

increment of 1.0 μ m. The refractive index dataset of water by Hale and Querry [28] is used in making the LUTs. The simulation results with $f=f_{\text{TA,fitted}}$ and $f_{p,\text{fitted}}$ are almost identical (not shown), and hence we only show the results with $f=f_{p,\text{fitted}}$ here. As compared to the δ -16-stream reference simulations, Figs. 6a and 7a show that the conventional δ -Eddington approach ($f=f_{g2}=g^2$) overestimates F_{TOA} and F_{SURF} at low solar elevations ($\theta_0 > 70^\circ$) in the optically

thin condition. In the optically thick condition, while Fig. 9a shows that the conventional δ -Eddington approach overestimates of $F_{\rm SURF}$ at low solar elevations ($\theta_0 > 80^{\circ}$), Fig. 8a shows that the $F_{\rm TOA}$ simulations by the conventional δ -Eddington approach generally agree with those by the δ -16-stream approach with relative errors less than 5% for most conditions. The success of the conventional δ -Eddington method in the optically thick regime and the degraded accuracy of the conventional δ -Eddington method at intermediate and small optical depths have been reported by previous studies (e.g., [15]).

As shown in Figs. 6b and 7b, the F_{TOA} and F_{SURF} simulations do not show overall improvement in terms of the RMSE, if $f=f_{g_2}=g^2$ is replaced by $f=f_{p,fitted}$ in the δ -Eddington method in optically thin condition. F_{TOA} is underestimated at low solar elevations (around $\theta_0=70^\circ$) in the method where $f=f_{p,fitted}$ (Fig. 6b). In Figs. 8b and 9b, F_{TOA} and F_{SURF} are greatly underestimated and overestimated, respectively, in the optically thick regime ($\tau>20$ in shortwave bands) in the method where $f=f_{p,fitted}$. The results suggest that although a truncation-angle-based separation of the forward and diffusive components may improve the estimation of the angular distribution of radiance [19], it does not appear that setting $f=f_p$ improves the flux calculations in the δ -Eddington method, particularly at large optical depths.

However, if we set f to the 3rd moment of the HG phase function (g^3), a measure of the phase function skewness, Fig. 6c shows

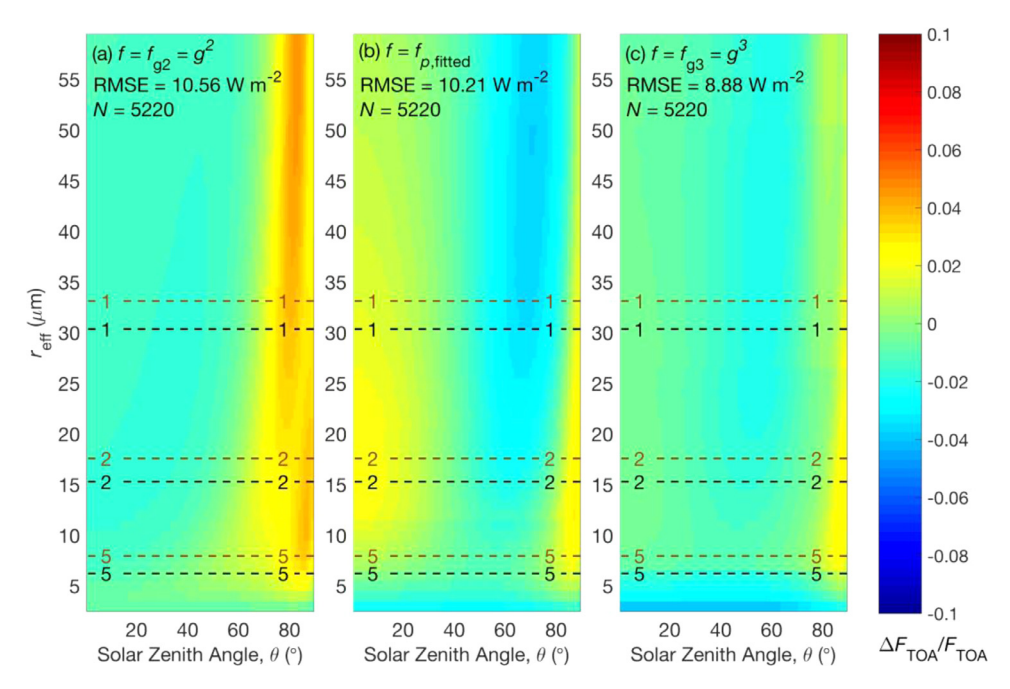


Fig. 6. The relative errors of the radiation fluxes at the TOA $(\Delta F_{TOA}/F_{TOA})$ for (a) $f = f_{g2} = g^2$, (b) $f = f_{p,fitted}$, and (c) $f = f_{g3} = g^2$ with the cloud water path fixed to 20 g m⁻². The dashed black and brown lines are the contours of the bands with minimum and maximum r_{eff} associated with the labeled optical thicknesses $(\tau) = 1$, 2, or 5 among the 14 RRTM_SW/RRTMG_SW bands, respectively. In each panel, RMSE is the root mean square error; N is the number of samples. The U.S. Standard Atmosphere, 1976, profile is used.

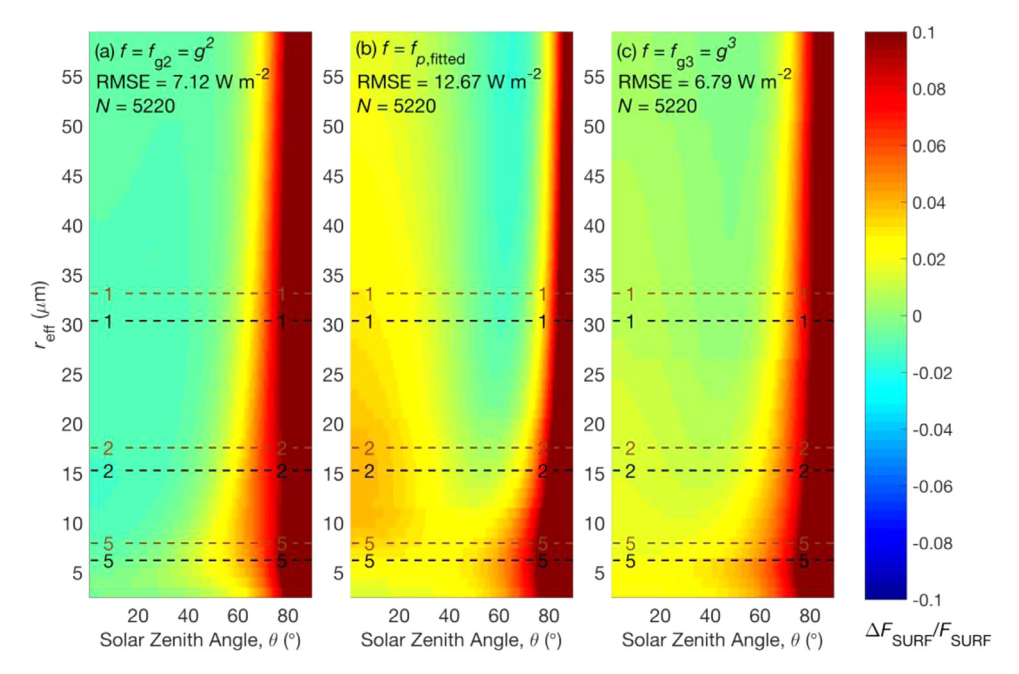


Fig. 7. Same as Fig. 6 except for the radiation fluxes at the surface ($\Delta F_{\text{SURF}}/F_{\text{SURF}}$).

that the $F_{\rm TOA}$ simulations improve in the optically thin regime with an RMSE reducing from 10.56 to 8.88 W m $^{-2}$ for the *U.S. Standard Atmosphere*, 1976. In Fig. 7c, with $f=g^3$ the $F_{\rm SURF}$ simulations also improve in the optically thin regime. The improvements of $F_{\rm TOA}$ and $F_{\rm SURF}$ at intermediate and small optical depths ($\tau < 5$ in shortwave bands) by setting $f=g^3$ also apply for other atmospheric profiles as documented in Table 2.

Figs. 8c and 9c show that the estimations of F_{TOA} and F_{SURF} are not improved with $f=g^3$ at large optical depths, however. The conventional δ -Eddington approximation ($f=g^2$) is more accurate than setting $f=g^3$ in optically thick conditions. This is because the multiple scattering is the dominant term in determining the re-

flectance (R) and transmittance (T) of an atmospheric layer. As long as the optical thickness is large, a large portion of the photons from the incident light will deviate from the original direction, no matter how strong the forward peak of the phase function is. It appears that the δ -Eddington phase function (forward + diffusive components) that shares the same variance (i.e. 2nd moment) with the original phase function is more accurate than the δ -Eddington phase function that shares the same skewness (i.e. 3rd moment) with the original phase function in such optically thick conditions. However, single scattering of the incident light becomes more important in determining R and T in optically thin conditions, making the parameterization of f using a measure of the skewness of phase

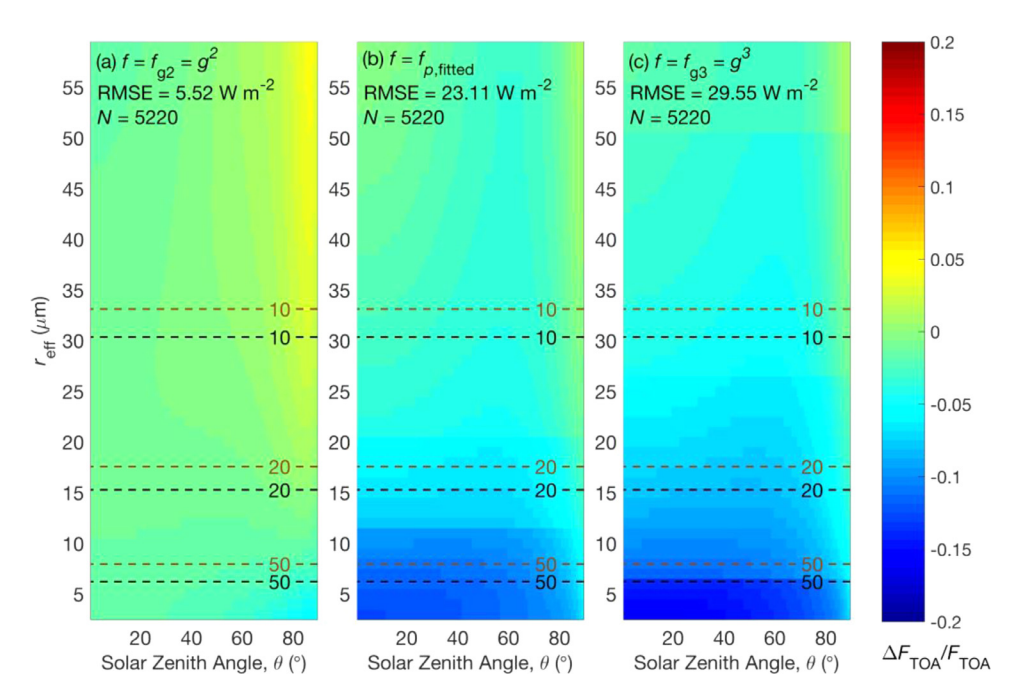


Fig. 8. Same as Fig. 6 except that the cloud water path is fixed to $200 \, \text{g m}^{-2}$.

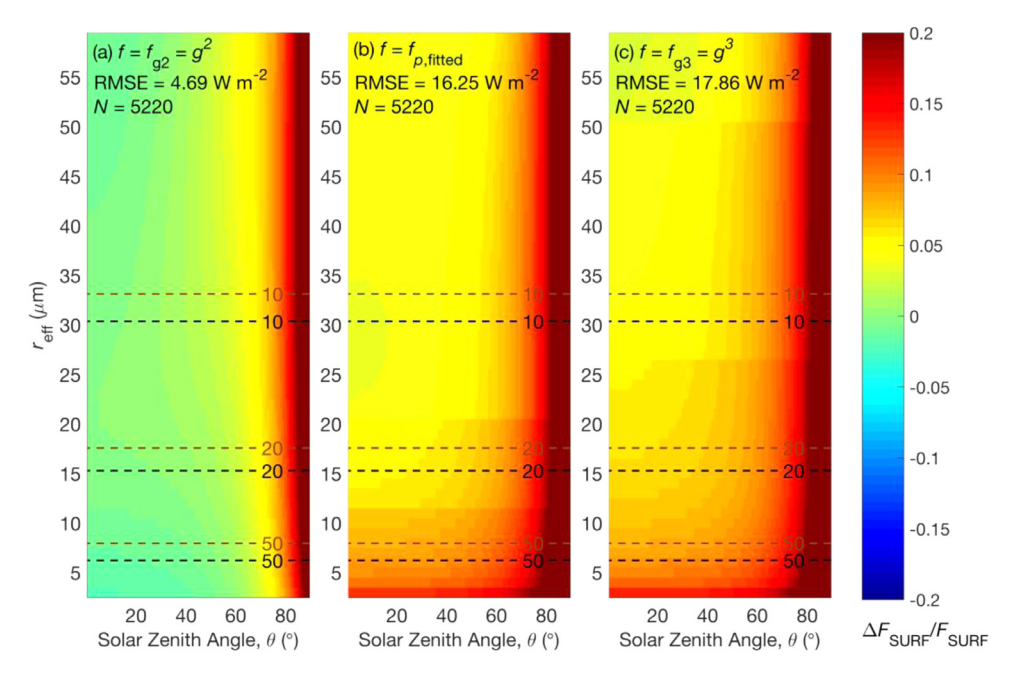


Fig. 9. Same as Fig. 7 except that the cloud water path is fixed to $200 \, \mathrm{g \ m^{-2}}$.

Table 2 RMSEs of $F_{\rm TOA}$ and $F_{\rm SURF}$ (W m $^{-2}$) for different parameterizations of f under different atmospheric conditions with the cloud water path fixed to 20 g m $^{-2}$.

Atmospheric	F_{TOA}			F _{SURF}			
profiles	f_{δ}	$f_{p,\mathrm{fitted}}$	$f_{ m g3}$	f_{δ}	$f_{p,\mathrm{fitted}}$	$f_{ m g3}$	
U.S. Standard Atmosphere	10.56	10.21	8.88	7.12	12.67	6.79	
Tropical	9.81	9.89	8.23	6.89	10.86	5.68	
Midlatitude summer	10.13	10.05	8.53	6.85	11.49	6.08	
Midlatitude winter	10.87	10.34	9.29	7.35	13.17	7.13	
Subarctic summer	10.38	10.09	8.70	6.97	12.20	6.49	
Subarctic winter	11.10	10.45	9.55	7.71	13.75	7.47	

function more accurate than that using a measure of the variance of the phase function.

It should be noted that although $f=g^3$ provides more accurate F_{TOA} and F_{SURF} simulations in optically thin conditions, setting $f=g^3$ results in a smaller heating rate within the cloud layer and generally larger heating rates below (not shown). The result suggests that $f=g^3$ tends to let more photons pass through the cloud layer. The conventional approach $f=g^2$ is the most accurate among the 3 parameterizations of $f(f_{g2}, f_{p,fitted}, \text{ and } f_{g3})$ in terms of the heating rate within the cloud layer (H_{cld}) or the heating rate of the atmospheric column that includes the cloud layer and below (H_{col}) . While the cloud longwave forcing impacts mostly on the atmospheric column, the cloud shortwave forcing is primarily felt by the surface (e.g., [47,48]). Hence, notwithstanding the degraded accuracy of H_{cld} and H_{col} , the resultant more accurate F_{TOA} and F_{SURF} make $f=g^3$ applicable to cloud shortwave forcing evalu-

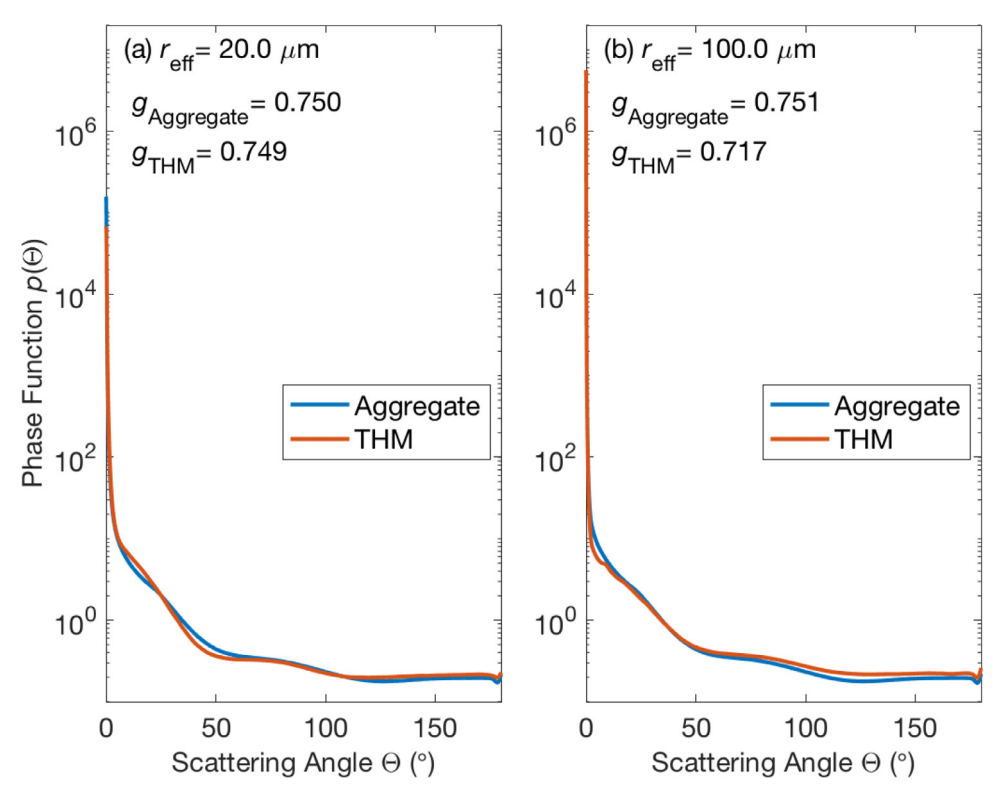


Fig. 10. Phase functions of the aggregate model and the THM in Band 25 (visible) of the RRTM_SW/RRTMG_SW for ice particles with effective radii of (a) $20.0\,\mu\text{m}$ and (b) $100.0\,\mu\text{m}$.

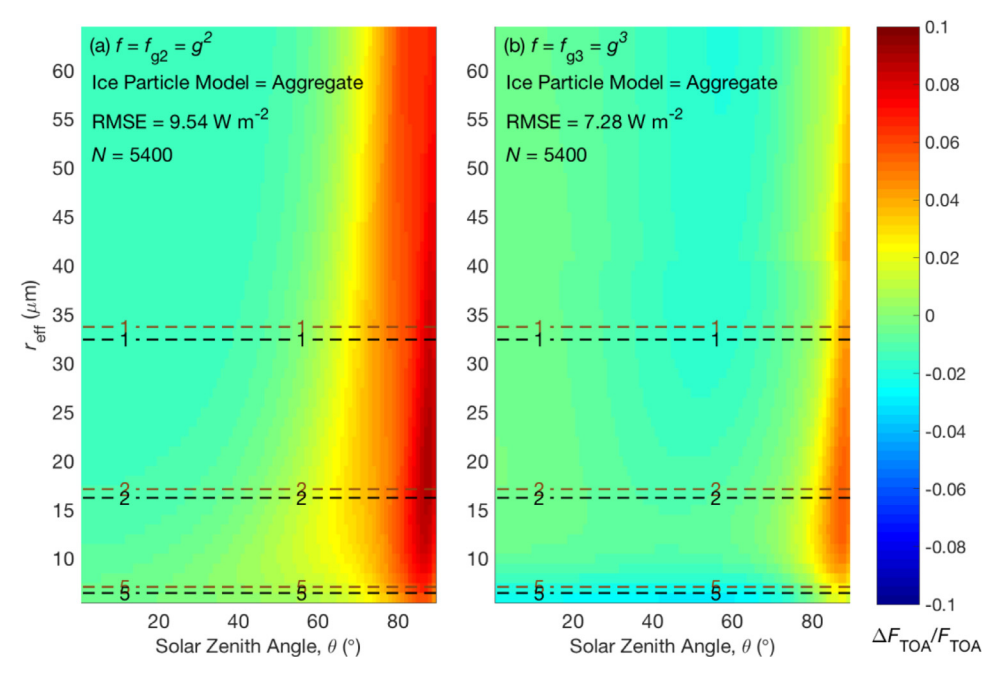


Fig. 11. The relative errors of the radiation fluxes at the TOA ($\Delta F_{\text{TOA}}/F_{\text{TOA}}$) for (a) $f = f_{\delta} = g^2$ and (b) $f = f_{\text{mom}3} = g^3$ with the ice water path fixed at 20 g m⁻² using the aggregate model. The dashed black and brown lines are the contours of the minimum and maximum cloud optical thicknesses (τ) among the 14 RRTM_SW/RRTMG_SW bands, respectively. The *U.S. Standard Atmosphere*, 1976, profile is used.

ations. We therefore suggest the following 3rd order Pade function as an improved parameterization of f for an atmosphere of cloud droplets:

 $f = f_{\text{Pade}} = \frac{g^3 + (\tau/2.5)^3 g^2}{1 + (\tau/2.5)^3}.$ (16)

The simulation results of F_{TOA} , F_{SURF} , and H_{col} with $f = f_{\text{Pade}}$ are omitted here and are available in the supplemental material.

3.2. $f = g^3$ for ice clouds

As previously shown, F_{TOA} and F_{SURF} can be computed more accurately in an optically thin atmosphere of liquid clouds by set-

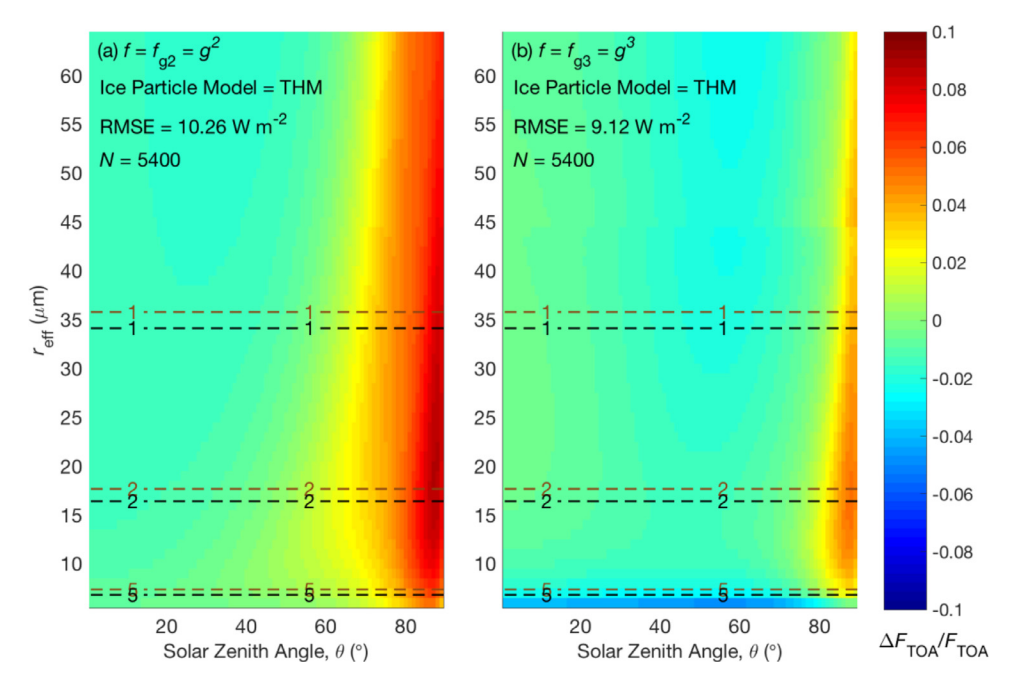


Fig. 12. Same as Fig. 11 except that the THM is used.

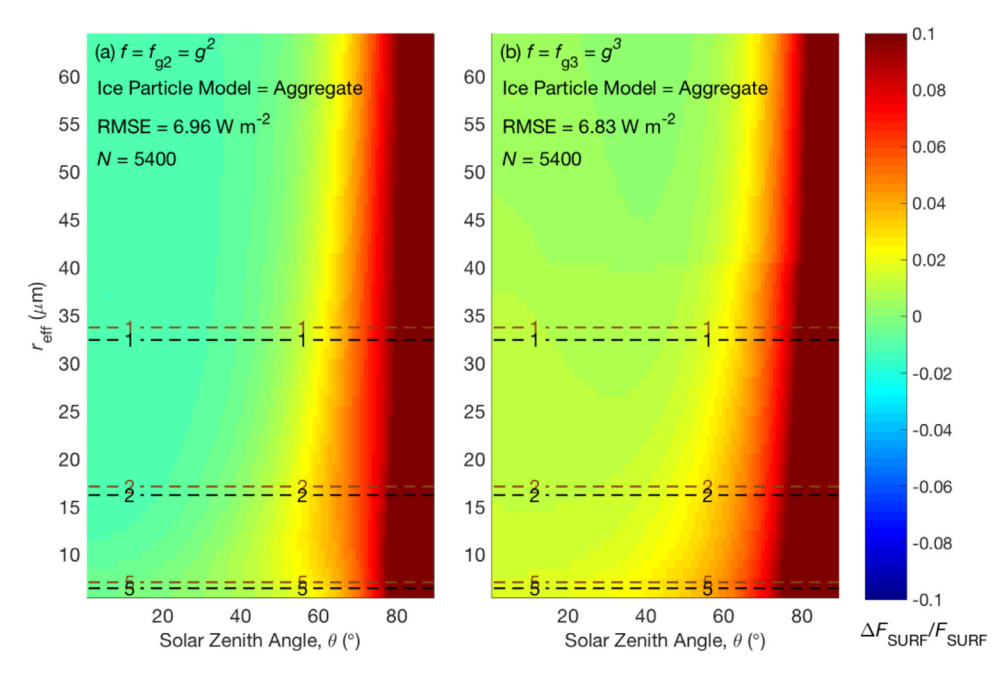


Fig. 13. Same as Fig. 11 except for the radiation fluxes at the surface $(\Delta F_{\text{SURF}}/F_{\text{SURF}})$.

ting $f=g^3$ in the δ -Eddington approximation. Here, we test this parameterization for ice clouds. Simulations of an atmosphere of ice clouds are conducted using RRTMG_SW and RRTM_SW for a number (129,600) of conditions documented in Table 3. Two recently developed ice particle models, the surface-roughened 8-hexagonal-column aggregate model (aggregate model hereinafter; [49]) and the two-habit model (THM; [50]) are added into the RRTMG_SW and RRTM_SW and adopted for the simulations. The aggregate model is used in the Moderate Resolution Imaging Spectroradiometer (MODIS) Collection 6 cloud retrievals [51]. The THM model consists of a surface-roughened single-hexagonal-column and a 20-column aggregate model with a specified increasing percentage of 20-column aggregates as the particle size increases [50]. The development of such a THM is motivated by the observational

evidence of increased complexity of ice particles with increasing particle size [52,53]. As reported by the previous study [50], one distinct feature of the THM is that g decreases as particle size increases at visible wavelengths because the fraction of fluffy particles that have a smaller g increases with increasing particle size in the THM. Fig. 10 shows examples of the phase function averaged over small ($r_{\rm eff} = 20 \, \mu \, \rm m$) and large ($r_{\rm eff} = 100 \, \mu \, \rm m$) particle sizes

To derive the bulk optical properties for each of the 14 bands of RRTM_SW/RRTMG_SW shown in Fig. 4, and assuming gamma size distributions with constant 0.1 effective variance, computations are performed for various values of $r_{\rm eff}$, which is defined as the ratio of the volume to the projected area of ice particles [54–56]. The same gamma size distribution is assumed in MODIS Collection 6 cloud

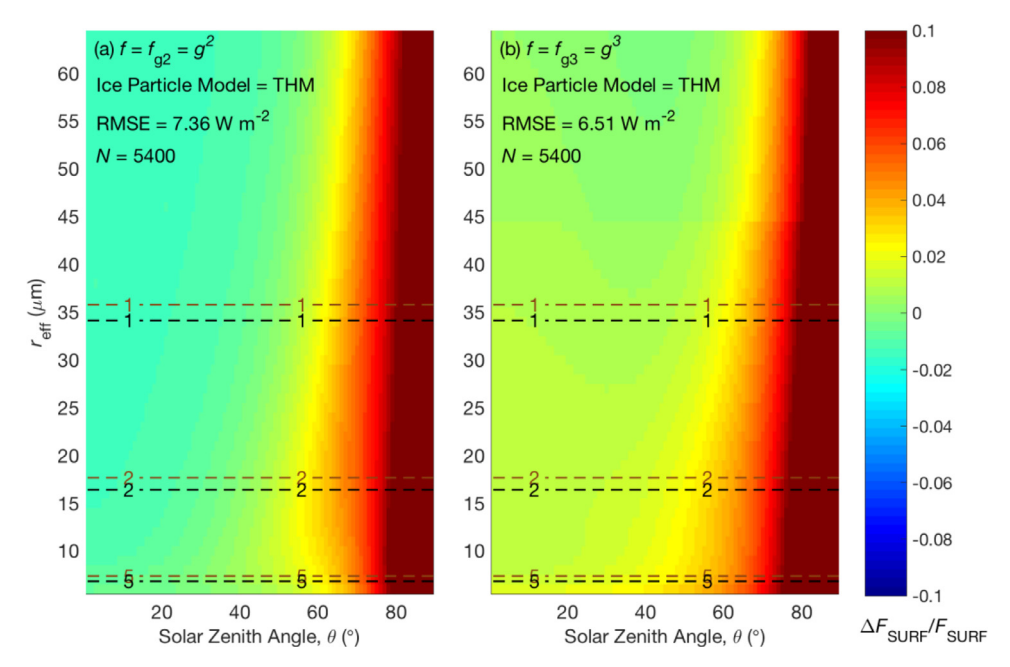


Fig. 14. Same as Fig. 13 except that the THM is used.

Table 3Selected conditions for the comparison simulations for ice clouds.

RRTMG_SW/RRTM_SW input parameters	Selected values (or options)				
Atmospheric profiles	U.S. Standard Atmosphere, 1976 Tropical				
	Midlatitude summer				
	Midlatitude winter				
	Subarctic summer				
	Subarctic winter				
Ice particle models	Aggregate model (Yang et al. 2013)				
	Two-habit model (Loeb et al. 2018)				
Cloud layer height (km)	Between 9.0 and 9.5 km				
Ice water paths (CWP; g m ⁻²)	20 and 200				
Solar zenith angles, θ_0 (°)	From 0.5 to 89.5 with an increment of 1.0				
Effective radii, $r_{\rm eff}$ (μ m)	From 5.5 to 64.5 with an increment of 1.0				
Surface albedo	0.2				

retrievals [51]. In each band, $\beta_{\rm ext}$, ω , and g are parameterized as functions of $r_{\rm eff}$ as follows:

$$\begin{cases} \beta_{\text{ext}}/\text{IWC} = A_1 r_{\text{eff}} + A_0 + \frac{A_{-1}}{r_{\text{eff}}} + \frac{A_{-2}}{r_{\text{eff}}^2} + \frac{A_{-3}}{r_{\text{eff}}^3} \\ 1 - \omega = B_1 r_{\text{eff}} + B_0 + \frac{B_{-1}}{r_{\text{eff}}} + \frac{B_{-2}}{r_{\text{eff}}^2} + \frac{B_{-3}}{r_{\text{eff}}^3} \\ g = C_1 r_{\text{eff}} + C_0 + \frac{C_{-1}}{r_{\text{eff}}} + \frac{C_{-2}}{r_{\text{eff}}^2} + \frac{C_{-3}}{r_{\text{eff}}^3} \end{cases}, \tag{17}$$

where IWC is ice water content (g m⁻³), and A_i , B_i , C_i (i = 1, 0, -1, -2, -3) are coefficients that are determined by a least-square. An ice density of 0.9167 g cm⁻³ is assumed [30].

As with the simulations of liquid clouds in Figs. 6–9 and Table 2, the simulations of ice clouds in Figs. 11–14 and Table 4 also suggest improved F_{TOA} and F_{SURF} , if $f=g^2$ is replaced by $f=g^3$ in the δ -Eddington approximation in optically thin conditions. The overestimations of F_{TOA} at low solar elevations ($\theta_0 > 70^\circ$) and the underestimations of F_{SURF} ($\theta_0 < 20^\circ$) at high solar elevations are reduced, if the 3rd order moments of the δ -Eddington phase function (forward+diffusive components) and original phase function are made the same, i.e. setting $f=g^3$. Table 4 shows that when $f=g^3$, F_{TOA} has smaller RMSEs for all 6 selected atmospheric profiles; F_{SURF} also has smaller RMSEs except for midlatitude and subarctic winter when the aggregate model is used. When ice clouds are optically thick, in agreement with the situations for liquid clouds (Figs. 8 and 9), setting $f=g^3$ is no better than the conven-

tional δ -Eddington approximation (not shown). Letting $f=g^3$ also results in a smaller heating rate within the cloud layer and generally larger heating rates below for ice clouds (not shown). The conventional approach $f=g^2$ is also the most accurate among the 3 parameterizations of $f(f_{g_2}, f_{p,fitted}, \text{ and } f_{g_3})$ in terms of H_{cld} and H_{col} calculations for ice clouds. Because the ice cloud layer is high, the cooling bias introduced by $f=g^3$ within the cloud layer is more or less compensated for by the warming bias below (not shown). Based on the improved simulations of F_{TOA} and F_{SURF} in the overcast conditions of optically thin ice clouds, we suggest that the parameterization in Eq. (16) should be used with both liquid and ice clouds. The simulation results of F_{TOA} , F_{SURF} , and H_{col} with $f=f_{\text{Pade}}$ for ice clouds are omitted here and available in the supplemental material.

4. Conclusions

The δ -scaling method has been used for solving shortwave radiative transfer in a highly anisotropic scattering atmosphere. In the conventional δ -Eddington approximation, f is set to g^2 , which is a measure of the variance of the phase function. As already reported by a previous study [15], the conventional approach $(f=g^2)$ shows accurate results for optically thick clouds $(\tau \geq 5)$. However, for the optically thin clouds $(\tau < 5)$, single scattering becomes

Table 4 RMSEs of F_{TOA} and F_{SURF} (W m⁻²) for different parameterizations of f under different atmospheric conditions with the ice water path fixed to 20 g m⁻², using the aggregate model and the two-habit model.

Atmospheric profiles	Aggregate model				Two-habit model			
	$\overline{F_{TOA}}$		F _{SURF}		F_{TOA}		F _{SURF}	
	$f_{\rm g2}$	$f_{\mathrm{g}3}$	$\overline{f_{\mathrm{g2}}}$	$f_{ m g3}$	$f_{\rm g2}$	$f_{ m g3}$	$\overline{f_{\mathrm{g2}}}$	$f_{\mathrm{g}3}$
U.S. Standard Atmosphere	9.54	7.28	6.96	6.83	10.26	9.12	7.36	6.51
Tropical	8.81	5.93	6.70	5.28	9.46	7.70	7.18	5.00
Midlatitude summer	9.08	6.57	6.67	5.90	9.78	8.38	7.12	5.58
Midlatitude winter	9.87	7.83	7.15	7.39	10.63	9.69	7.54	7.07
Subarctic summer	9.31	6.81	6.79	6.41	10.02	8.66	7.25	6.08
Subarctic winter	10.19	8.45	7.49	7.92	10.97	10.33	7.89	7.61

more important than multiple scattering in determining the R and T of a cloudy layer, and the conventional approach $(f=g^2)$ shows biased F_{TOA} and F_{SURF} at low solar elevations. Hence, g^2 may not be a best parameterization for f for optically thin clouds. This study tests other parameterizations of f for optically thin clouds, including (1) the ratio of the forward single-scattered intensity to the total single-scattered intensity (f_p) and (2) the cube of the asymmetry factor (g^3) . f_p is evaluated based on the truncation angle method [19]. The results show that $f_p < g^3 < g^2$ in the whole shortwave region, and hence the scaled asymmetry factor (g) satisfies $g(f=g^2) < g(f=g^3) < g(f=f_p)$. In other words, both $f=g^3$ and $f=f_p$ make the diffusive part of the phase function more asymmetric than the conventional approach $(f=g^2)$. We show that F_{TOA} and F_{SURF} calculations are more accurate for both liquid and ice clouds in optically thin conditions (τ < 5) if f is set to g^3 , which is a measure of the skewness of the phase function. In addition, setting $f=g^3$ also brings errors to the heating rates within the cloud layer and below. The conventional approach $f=g^2$ is most accurate in calculating the heating rates among the 3 parameterizations ($f = g^2$, $f = f_p$, and $f = g^3$). The δ -Eddington phase function (forward + diffusive components) with $f = g^2$ keeps the original 2rd order moment; the δ -Eddington phase function with $f = g^3$ keeps the original 3rd order moment but has the diffusive component more asymmetric. We suggest an improved parameterization of f(Eq. (16)) in the shortwave bands for a cloudy atmosphere. The application of the suggested parameterization will improve the estimation of cloud shortwave forcing that is mainly observable at the surface (e.g., [47,48]), particularly for the generally thin cirrus clouds (e.g., [57]). The improved parameterization of f can likely be straightforwardly extended for aerosol particles whose scattering phase functions are also asymmetric (e.g., [3]). However, although the optical thickness of an aerosol layer is usually small (e.g., [58,59]), the optical thickness threshold where $f = g^3$ provides a more accurate δ -Eddington approximation than $f = g^2$ needs to be investigated for aerosol particles in future studies.

Declaration of Competing Interest

This manuscript does not have any conflict of interest issues.

Acknowledgments

This study was supported by the National Science Foundation (AGS-1632209). T. Ren appreciates his discussions of the results in this work with Dr. Jiachen Ding, Dr. Masanori Saito, and Dr. Steve Schroeder. We also thank the Texas A&M High Performance Research Computing for providing the disk quota and software for the simulations in this study.

Supplementary materials

Supplementary material associated with this article can be found, in the online version, at doi:10.1016/j.jqsrt.2019.106694.

References

- [1] Joseph JH, Wiscombe W, Weinman J. The delta-Eddington approximation for radiative flux transfer. J Atmos Sci 1976;33:2452–9 doi:10.1175/1520-0469(1976)033(2452:TDEAFR)2.0.CO;2.
- [2] Meador W, Weaver W. Two-stream approximations to radiative transfer in planetary atmospheres: a unified description of existing methods and a new improvement. J Atmos Sci 1980;37:630–43 doi:10.1175/1520-0469(1980) 037(0630:TSATRT)2.0.CO;2.
- [3] Mishchenko MI, Travis LD, Kahn RA, West RA. Modeling phase functions for dustlike tropospheric aerosols using a shape mixture of randomly oriented polydisperse spheroids. J Geophys Res 1997;102:16831–47. doi:10.1029/ 96ID02110
- [4] Yang P, Liou K-N, Bi L, Liu C, Yi B, Baum BA. On the radiative properties of ice clouds: light scattering, remote sensing, and radiation parameterization. Adv Atmos Sci 2015;32:32–63. doi:10.1007/s00376-014-0011-z.
- [5] Yang P, Hong G, Dessler AE, Ou SS, Liou K-N, Minnis P, et al. Contrails and induced cirrus: optics and radiation. Bull Am Meteorol Soc 2010;91:473–8. doi:10.1175/2009BAMS2837.1.
- [6] Wiscombe W. The Delta-M method: rapid yet accurate radiative flux calculations for strongly asymmetric phase functions. J Atmo Sci 1977;34:1408-22 doi:10.1175/1520-0469(1977)034(1408:TDMRYA)2.0.CO;2.
- [7] Shettle E, Weinman J. The transfer of solar irradiance through inhomogeneous turbid atmospheres evaluated by Eddington's approximation. J Atmos Sci 1970;27:1048–55. doi:10.1175/1520-0469(1970)027(1048:TTOSIT)2.0.CO;2.
- [8] Liou K-N. A numerical experiment on Chandrasekhar's discrete-ordinate method for radiative transfer: applications to cloudy and hazy atmospheres. J Atmos Sci 1973;30:1303–26. doi:10.1175/1520-0469(1973)030(1303:ANEOCD) 2.0.CO;2.
- [9] van de Hulst HC. The spherical albedo of a planet covered with a homogeneous cloud layer. Astron Astrophys 1974;35:209.
- [10] Zdunkowski W, Welch R, Korb G. An investigation of the structure of typical two-stream-methods for the calculation of solar fluxes and heating rates in clouds. Beiträge Phy Atmos 1980;53:147–66.
- [11] Boucher O, Schwartz So, Ackerman T, Anderson T, Bergstrom B, Bonnel B, et al. Intercomparison of models representing direct shortwave radiative forcing by sulfate aerosols. J Geophys Res 1998;103:16979–98. doi:10.1029/98JD00997.
- [12] Fouquart Y, Bonnel B, Ramaswamy V. Intercomparing shortwave radiation codes for climate studies. J Geophys Res 1991;96:8955–68. doi:10.1029/ 90ID00290.
- [13] Randles CA, Kinne S, Myhre G, Schulz M, Stier P, Fischer J, et al. Intercomparison of shortwave radiative transfer schemes in global aerosol modeling: results from the aerocom radiative transfer experiment. Atmos Chem Phys 2013:13:2347-79. doi:10.5194/acp-13-2347-2013.
- [14] Räisänen P. Two-stream approximations revisited: a new improvement and tests with GCM data. Q J R Meteorol Soc 2002;128:2397–416. doi:10.1256/qj. 01.161
- [15] King MD, Harshvardhan. Comparative accuracy of selected multiple scattering approximations. J Atmos Sci 1986;43:784–801. doi:10.1175/1520-0469(1986) 043/0784:CAOSMS)2.0.CO;2.
- [16] Li J. On the fractional scattering into the forward peak. J Atmos Sci 1999;56:2728–32. doi:10.1175/1520-0469(1999)056(2728:0TFSIT)2.0.CO;2.
- [17] Qiu J. Modified delta-Eddington approximation for solar reflection, transmission, and absorption calculations. J Atmos Sci 1999;56:2955–61. doi:10.1175/1520-0469(1999)056(2955:MDEAFS)2.0.CO;2.
- [18] Chaikovskaya L, Katsev I, Prikhach A, Zege E. Fast code to compute polarized radiation transfer in the atmosphere-ocean and atmosphere-earth systems. Proc IEEE 1999;2 1398-00.

- [19] Sun B, Kattawar GW, Yang P, Mlawer E. An improved small-angle approximation for forward scattering and its use in a fast two-component radiative transfer method. J Atmos Sci 2017;74:1959–87. doi:10.1175/JAS-D-16-0278.1.
- [20] Budak V, Ilyushin YA. Development of the small angle approximation of the radiative transfer theory taking into account the photon path distribution function. Atmos Oceanic Opt 2010:23:181–5. doi:10.1134/S1024856010030048.
- [21] Lenoble J, Herman M, Deuzé J, Lafrance B, Santer R, Tanré D. A successive order of scattering code for solving the vector equation of transfer in the earth's atmosphere with aerosols. J Quant Spectrosc Radiat Transf 2007;107:479–507. doi:10.1016/j.jqsrt.2007.03.010.
- [22] Min Q, Duan M. A successive order of scattering model for solving vector radiative transfer in the atmosphere. J Quant Spectrosc Radiat Transf 2004;87:243–59. doi:10.1016/j.jqsrt.2003.12.019.
- [23] Myneni R, Asrar G, Kanemasu E. Light scattering in plant canopies: the method of successive orders of scattering approximations (SOSA). Agric For Meteorol 1987;39:1–12. doi:10.1016/0168-1923(87)90011-6.
- [24] Zhai P-W, Hu Y, Trepte CR, Lucker PL. A vector radiative transfer model for coupled atmosphere and ocean systems based on successive order of scattering method. Opt Express 2009;17:2057–79. doi:10.1364/0E.17.002057.
- [25] Morrison H, Gettelman A. A new two-moment bulk stratiform cloud microphysics scheme in the community atmosphere model, version 3 (CAM3). Part I: description and numerical tests. J Clim 2008;21:3642–59. doi:10.1175/ 2008/CI12105.1
- [26] Martin G, Johnson D, Spice A. The measurement and parameterization of effective radius of droplets in warm stratocumulus clouds. J Atmos Sci 1994;51:1823–42. doi:10.1175/1520-0469(1994)051(1823:TMAPOE)2.0.CO;2.
- [27] Bohren CF, Huffman DR. Absorption and scattering of light by small particles John Wiley & Sons; 2008.
- [28] Hale GM, Querry MR. Optical constants of water in the 200-nm to 200- μ m wavelength region. Appl Opt 1973;12:555–63. doi:10.1364/A0.12.000555.
- [29] Garrett TJ. Observational quantification of the optical properties of cirrus cloud. In: Light scattering reviews 3. Springer; 2008. p. 3–26.
- [30] Fu Q. An accurate parameterization of the solar radiative properties of cirrus clouds for climate models. J Clim 1996;9:2058–82. doi:10.1175/1520-0442(1996)009(2058:AAPOTS)2.0.CO;2.
- [31] Hu Y, Stamnes K. An accurate parameterization of the radiative properties of water clouds suitable for use in climate models. J Clim 1993;6:728–42. doi:10. 1175/1520-0442(1993)006(0728:AAPOTR)2.0.CO;2.
- [32] Yang P, Wei H, Huang H-L, Baum BA, Hu YX, Kattawar GW, et al. Scattering and absorption property database for nonspherical ice particles in the nearthrough far-infrared spectral region. Appl Opt 2005;44:5512–23. doi:10.1364/ AO 44.005512
- [33] Mlawer EJ, Taubman SJ, Brown PD, Iacono MJ, Clough SA. Radiative transfer for inhomogeneous atmospheres: RRTM, a validated correlated-k model for the longwave. J Geophys Res 1997;102:16663–82. doi:10.1029/97JD00237.
- [34] Clough S, Shephard M, Mlawer E, Delamere J, Iacono M, Cady-Pereira K, et al. Atmospheric radiative transfer modeling: a summary of the AER codes. J Quant Spectrosc Radiat Transf 2005;91:233–44. doi:10.1016/j.jqsrt.2004.05.058.
- [35] Iacono MJ, Delamere JS, Mlawer EJ, Shephard MW, Clough SA, Collins WD. Radiative forcing by long-lived greenhouse gases: calculations with the AER radiative transfer models. J Geophysic Res 2008;113. doi:10.1029/2008JD009944.
- [36] Kay J, Deser C, Phillips A, Mai A, Hannay C, Strand G, et al. The community earth system model (CESM) large ensemble project: a community resource for studying climate change in the presence of internal climate variability. Bull Am Meteorol Soc 2015;96:1333–49. doi:10.1175/BAMS-D-13-00255.1.
- [37] Powers JG, Klemp JB, Skamarock WC, Davis CA, Dudhia J, Gill DO, et al. The weather research and forecasting model: overview, system efforts, and future directions. Bull Am Meteorol Soc 2017;98:1717–37. doi:10.1175/ BAMS-D-15-00308.1.
- [38] Skamarock WC, Klemp JB, Dudhia J, Gill DO, Barker DM, Duda MG, et al. A description of theadvanced research WRF version 3; 2008. NCAR Tech Note NCAR/TN-475+STR p. 1–96.
- [39] Nakajima T, Tanaka M. Algorithms for radiative intensity calculations in moderately thick atmospheres using a truncation approximation. J Quant Spectrosc Radiat Transf 1988;40:51–69. doi:10.1016/0022-4073(88)90031-3.

- [40] Stamnes K, Tsay S-C, Wiscombe W, Jayaweera K. Numerically stable algorithm for discrete-ordinate-method radiative transfer in multiple scattering and emitting layered media. Appl Opt 1988;27:2502–9. doi:10.1364/AO.27.002502
- [41] Kuo CP, Yang P, Huang X, Feldman D, Flanner M, Kuo C, et al. Impact of multiple scattering on longwave radiative transfer involving clouds. J Adv Model Earth Syst 2017;9:3082–98. doi:10.1002/2017MS001117.
- [42] Tang G, Yang P, Kattawar GW, Huang X, Mlawer EJ, Baum BA, et al. Improvement of the simulation of cloud longwave scattering in broadband radiative transfer models. J Atmos Sci 2018;75:2217–33. doi:10.1175/JAS-D-18-0014.1.
- [43] Chou M-D, Lee K-T, Tsay S-C, Fu Q. Parameterization for cloud longwave scattering for use in atmospheric models. J Clim 1999;12:159–69. doi:10.1175/ 1520-0442-12.1.159.
- [44] McKellar BH, Box MA. The scaling group of the radiative transfer equation. J Atmos Sci 1981;38:1063–8. doi:10.1175/JAS-D-18-0014.1.
- [45] Turner DD. Arctic mixed-phase cloud properties from AERI lidar observations: algorithm and results from SHEBA. J Appl Meteorol 2005;44:427-44. doi:10. 1175/JAM2208.1.
- [46] Turner DD, Ackerman S, Baum B, Revercomb HE, Yang P. Cloud phase determination using ground-based AERI observations at SHEBA. J Appl Meteorol 2003;42:701–15. doi:10.1175/1520-0450(2003)042 (0701:CPDUGA) 2.0.CO;2.
- [47] Ramanathan V. The role of earth radiation budget studies in climate and general circulation research. J Geophys Res 1987;92:4075–95. doi:10.1029/ |D092iD04p04075.
- [48] Slingo A, Slingo J. The response of a general circulation model to cloud longwave radiative forcing. I: introduction and initial experiments. Q J R Meteorol Soc 1988;114:1027–62. doi:10.1002/qj.49711448209.
- [49] Yang P, Bi L, Baum BA, Liou K-N, Kattawar GW, Mishchenko MI, et al. Spectrally consistent scattering, absorption, and polarization properties of atmospheric ice crystals at wavelengths from 0.2 to 100

 µm. J Atmos Sci 2013;70:330–47. doi:10.1175/JAS-D-12-039.1.
- [50] Loeb NG, Yang P, Rose FG, Hong G, Sun-Mack S, Minnis P, et al. Impact of ice cloud microphysics on satellite cloud retrievals and broadband flux radiative transfer model calculations. J Clim 2018;31:1851–64. doi:10.1175/ ICIJ-D-17-0426.1.
- [51] Platnick S, Meyer KG, King MD, Wind G, Amarasinghe N, Marchant B, et al. The MODIS cloud optical and microphysical products: collection 6 updates and examples from Terra and Aqua. IEEE Trans Geosci Remote Sens 2017;55:502– 25. doi:10.1109/TGRS.2016.2610522.
- [52] Liu C, Yang P, Minnis P, Loeb N, Kato S, Heymsfield A, et al. A two-habit model for the microphysical and optical properties of ice clouds. Atmos Chem Phys 2014;14:13719–37. doi:10.5194/acp-14-13719-2014.
- [53] Schmitt CG, Heymsfield AJ. Observational quantification of the separation of simple and complex atmospheric ice particles. Geophys Res Lett 2014;41:1301– 7. doi:10.1002/2013GL058781.
- [54] Foot J. Some observations of the optical properties of clouds. II: cirrus. Q J R Meteorol Soc 1988;114:145–64. doi:10.1002/qj.49711447908.
- [55] Hansen JE, Travis LD. Light scattering in planetary atmospheres. Space Sci Rev 1974;16:527–610. doi:10.1007/BF00168069.
- [56] Schumann U, Mayer B, Gierens K, Unterstrasser S, Jessberger P, Petzold A, et al. Effective radius of ice particles in cirrus and contrails. J Atmos Sci 2011;68:300–21. doi:10.1175/2010JAS3562.1.
- [57] Dowling DR, Radke LF. A summary of the physical properties of cirrus clouds. J Appl Meteorol 1990;29:970–8. doi:10.1175/1520-0450(1990) 029(0970:ASOTPP)2.0.CO;2.
- [58] Chu DA, Kaufman Y, Zibordi G, Chern J, Mao J, Li C, et al. Global monitoring of air pollution over land from the earth observing system-terra moderate resolution imaging spectroradiometer (MODIS). J Geophys Res 2003;108. doi:10.1029/2002/D003179.
- [59] Levy RC, Remer LA, Dubovik O. Global aerosol optical properties and application to moderate resolution imaging spectroradiometer aerosol retrieval over land. J Geophys Res 2007;112. doi:10.1029/2006JD007815.